

# Noise-Resilient 1SDI-QKD for Practical Quantum Networks

Syed M. Arslan\*, Muhammad T. Rahim\*, Asad Ali\*, Hashir Kuniyil, Saif Al-Kuwari\*

\*Qatar Center for Quantum Computing, HBKU, Doha, Qatar

**Abstract**—One-sided device-independent quantum key distribution (1SDI-QKD) offers a practical middle ground between fully device-independent protocols and standard QKD, achieving security with detection efficiencies as low as 50.1% on the untrusted side. However, prior analyses assumed idealized channels, neglecting realistic noise sources. We extend the 1SDI-QKD framework to include amplitude damping, dephasing, and depolarizing noise, quantifying their impact on secure key rates and efficiency requirements. Our results reveal a clear noise hierarchy: dephasing is most tolerable (secure keys achievable at 70% efficiency with 30% noise), while amplitude damping and depolarizing noise dramatically elevate requirements to over 90%. Crucially, we find that security is lost while substantial entanglement remains (concurrence  $C \approx 0.7\text{--}0.8$ ), demonstrating that steering violation, not merely entanglement, determines 1SDI-QKD security. To mitigate noise effects, we integrate the BBPSSW entanglement purification protocol, showing that 2–4 rounds can restore positive key rates in otherwise insecure regimes. Our resource overhead analysis reveals that effective key rates peak at moderate purification depths; excessive rounds become counterproductive. These findings establish practical boundaries for deploying 1SDI-QKD over metropolitan-scale quantum networks.

## I. INTRODUCTION

Quantum key distribution (QKD) allows two distant parties (Alice and Bob) to establish a shared secret key guaranteed by quantum physics rather than computational assumptions. Classical cryptographic protocols, which rely on computational hardness, face potential vulnerabilities with advancing algorithms and the advent of quantum computing [1], [2]. In contrast, QKD protocols like BB84 [3] offer unconditional security under idealized device models. Real-world devices, however, inevitably deviate from their ideal specifications, leading to potential security loopholes and side-channel attacks [4]. In fact, practical QKD implementations have been compromised by attacks exploiting detector imperfections, as exemplified by bright-light hacking of commercial systems [5]. These vulnerabilities motivate the development of QKD schemes that remain secure even when devices are uncharacterized and untrusted. Device-independent QKD addresses device-trust issues by certifying security from the observed violation of a Bell inequality under minimal assumptions (quantum/no-signaling, independent random choices, and secure labs). In a DI-QKD protocol, the devices are treated as black boxes, and a secret key can be established if the measurement correlations violate a Bell inequality by a sufficient margin [6]. This approach is robust against a wide range of device flaws or malicious behavior. However, fully DI-QKD has demanding requirements: detection efficiencies must be

extremely high (often well above 80%) and channel noise and losses minimal to avoid the detection loophole [7]. In practice, such conditions are difficult to achieve over long distances. Therefore, DI-QKD experiments were limited to laboratory-scale distances (meters) despite significant advances [6]. An alternative approach to overcoming detector-side vulnerabilities is measurement-device-independent QKD (MDI-QKD), which removes trust from detection by employing an untrusted intermediary to perform a Bell-state measurement on photons from Alice and Bob. MDI-QKD effectively closes all detector side channels and has been successfully demonstrated over long fiber distances, establishing it as a practical candidate for near-term QKD networks [8]. Nonetheless, MDI-QKD still requires trusted source devices that emit the prescribed quantum states, and thus it is not fully ‘device independent’ in the Bell-test sense. In particular, the users must trust their state preparation, and no Bell inequality is violated during key exchange. Therefore, fully DI-QKD remains the ultimate goal for device-untrusted security, but its experimental feasibility is currently limited by the stringent efficiency requirements. To bridge the gap between the strong security of DI-QKD and the practicality of standard QKD, one-sided device-independent (1SDI) QKD protocols have been developed. In a 1SDI scenario, only one of the two devices (e.g. Alice’s detection system) is assumed to be trusted and well-characterized, while the other device (Bob’s) is treated as a black box. This asymmetric trust significantly relaxes the requirements: security can be certified through an EPR-steering test, where Alice’s trusted measurements and the resulting correlations serve to verify the entanglement and “steerability” of Bob’s outcomes. Notably, Branciard et al. [9] proved that quantum steering (the phenomenon underlying 1SDI security) is both necessary and sufficient for secure key distribution in this setting. Recent “receiver-device-independent” QKD protocols [10] similarly assume an asymmetric trust and have mainly been studied in prepare-and-measure settings; our work complements these by focusing on an entanglement-based scheme and explicitly quantifying noise effects and purification gains.

By leveraging steering inequalities instead of full Bell inequalities, 1SDI-QKD tolerates much lower detector efficiency on Bob’s side. In this regard, a recent theoretical work by Masini and Sarkar [11] demonstrated a 1SDI protocol (with two measurement settings per party) secure against general coherent attacks with 50.1% detection efficiency at Bob’s side, close to the fundamental limit for any two-setting DI protocol. Despite this substantial improvement, prior security

analyses of 1SDI-QKD have largely assumed idealized conditions aside from photon loss. In contrast, we incorporate realistic quantum noise models (called amplitude damping, dephasing, and depolarizing channels noises) and due to which we confirm the entanglement sudden death (directly translates into loss of secure key) that had not been analyzed previously in this context. These noises are prevalent in practical fiber-optic and free-space quantum links and must be accounted for to accurately evaluate the viability of 1SDI-QKD in real networks. We find these quantum noises significantly raises the efficiency requirements, often demanding efficiencies above 90%, thereby providing a more realistic assessment of 1SDI-QKD performance in real-world scenarios. As a countermeasure, we integrate the BBPSSW entanglement purification protocol [12] into the 1SDI framework. To our knowledge, this is the first demonstration that shows the entanglement purification can effectively mitigate noise-induced efficiency demands on the untrusted party, enabling secure key rates in regimes that would otherwise yield no key generation. Our work highlights a promising direction for making 1SDI-QKD more resilient and deployable, while also revealing practical trade-offs and limitations of purification in noisy quantum networks.

#### A. Contributions

We provide the first comprehensive noise analysis of 1SDI-QKD under realistic channel conditions:

- 1) **Noise characterization:** We quantify how amplitude damping, dephasing, and depolarizing channels affect secure key rates and detection efficiency thresholds, identifying parameter regimes enabling positive key generation.
- 2) **Security-entanglement gap:** We demonstrate that key rates vanish before entanglement does for amplitude damping ( $\gamma \approx 0.36$  with  $C \approx 0.80$ ) and depolarizing noise ( $q \approx 0.24$  with  $C \approx 0.68$ ), revealing that sufficient steering violation—not merely entanglement—determines security.
- 3) **Purification analysis:** We integrate the BBPSSW protocol and demonstrate its efficacy in restoring security, while providing resource overhead analysis showing that effective key rates peak at 2–4 rounds.
- 4) **Operational guidelines:** We provide practical recommendations for deploying 1SDI-QKD over noisy channels.

In the following, Section II presents the theoretical framework for the 1SDI-QKD protocol, including state preparation, measurement choices, noise modeling, and key rate calculation. Section III introduces the three quantum noise channels studied. Section IV reports simulation results for secure key rates under varying noise and detector efficiencies, as well as the effects of initial entanglement. Section V evaluates the efficacy of entanglement purification (BBPSSW) in improving fidelity and key rates, including a summary table of key rate improvements versus purification rounds. We then provide a

Conclusion summarizing our contributions, a brief Outlook on experimental implementation and future work.

## II. PRELIMINARIES

In this section, we establish the mathematical framework for analyzing one-sided device-independent QKD security. We define the entropy measures that quantify information leakage, introduce concurrence as our entanglement metric, and establish notation used throughout this work.

### A. Asymptotic Key Rate

The security of QKD protocols is quantified by the secret key rate, the number of secure key bits extractable per quantum signal. In the asymptotic limit of infinitely many signals, the Devetak-Winter bound [13] establishes that the secure key rate satisfies

$$r_\infty \geq H(A_1|E) - H(A_1|B_1), \quad (1)$$

where  $H(A_1|E)$  quantifies Eve's uncertainty about Alice's measurement outcomes, and  $H(A_1|B_1)$  represents Bob's uncertainty about Alice's outcomes given his own measurement results. A positive value indicates that secure key bits can be distilled; when this quantity becomes negative, no secure key generation is possible.

The two terms have distinct physical interpretations:

- $H(A_1|E)$ : The conditional von Neumann entropy characterizing how much information an eavesdropper lacks about Alice's raw key bits. Higher values indicate better security.
- $H(A_1|B_1)$ : The conditional Shannon entropy quantifying the classical correlation between Alice and Bob. Lower values indicate stronger correlations, benefiting key generation.

### B. Entropy Calculations

1) **Bob's Uncertainty  $H(A_1|B_1)$ :** The conditional entropy between Alice's and Bob's measurement outcomes can be directly estimated from observed statistics. For measurement settings  $x = 1$  (Alice) and  $y = 1$  (Bob), it is defined as

$$H(A_1|B_1) = - \sum_{a,b} p(a,b|1,1) \log_2 \frac{p(a,b|1,1)}{p(b|1)}, \quad (2)$$

where  $p(a,b|1,1)$  is the joint probability of Alice obtaining outcome  $a$  and Bob obtaining outcome  $b$  when both use measurement setting 1, and  $p(b|1) = \sum_a p(a,b|1,1)$  is Bob's marginal probability. Equivalently, this can be written as

$$H(A_1|B_1) = H(A_1, B_1) - H(B_1), \quad (3)$$

where  $H(A_1, B_1)$  is the joint entropy and  $H(B_1)$  is Bob's marginal entropy.

2) **Eve's Uncertainty  $H(A_1|E)$ :** Bounding Eve's uncertainty is more challenging since her attack strategy and quantum side information are unknown. In device-independent settings, we employ two complementary approaches:

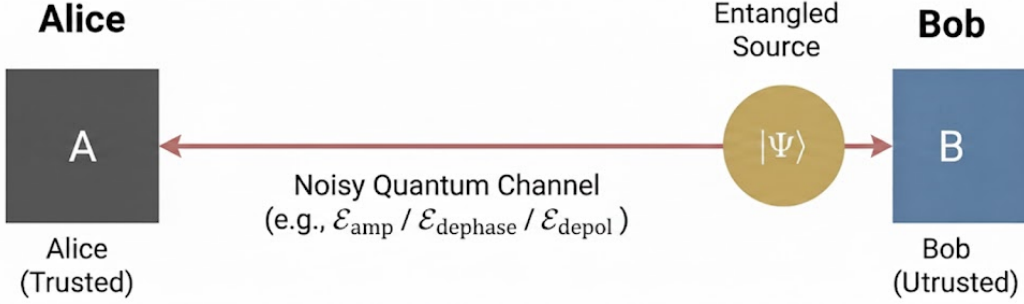


Fig. 1: Schematic of the one-sided device-independent QKD setup. An entangled source prepares the two-qubit state  $|\Psi\rangle$  and distributes one qubit to Alice (trusted) and the other to Bob (untrusted) through a noisy quantum channel characterized by amplitude-damping  $\mathcal{E}_{amp}$ , dephasing  $\mathcal{E}_{deph}$ , or depolarizing  $\mathcal{E}_{depol}$  noise.

*a) Analytical bounds.:* For specific protocol structures, closed-form bounds can be derived relating  $H(A_1|E)$  to observable quantities such as the steering parameter or CHSH value. Branciard *et al.* [9] established that for one-sided device-independent protocols, steering inequality violations directly bound Eve's information.

*b) Numerical optimization.:* The Brown-Fawzi-Fawzi (BFF) method [14], [15] provides tighter bounds by formulating  $H(A_1|E)$  as a solution to a noncommutative polynomial optimization problem. This is implemented via the Navascués-Pironio-Acín (NPA) hierarchy [16] of semidefinite programs, which yields a converging sequence of lower bounds on the conditional von Neumann entropy. In our analysis, we employ NPA level 2 with additional constraints reflecting Alice's measurement anti-commutativity.

### C. Concurrence as Entanglement Measure

To track how channel noise degrades the shared quantum state, we employ Wootters' concurrence [17] as our entanglement measure. For a two-qubit density matrix  $\rho$ , define the spin-flipped state

$$\tilde{\rho} = (\sigma_y \otimes \sigma_y) \rho^* (\sigma_y \otimes \sigma_y), \quad (4)$$

where  $\rho^*$  denotes complex conjugation in the computational basis. Let  $\{\lambda_i\}_{i=1}^4$  be the eigenvalues of the product  $\rho \tilde{\rho}$  arranged in non-increasing order. The concurrence is then

$$C(\rho) = \max \left\{ 0, \sqrt{\lambda_1} - \sqrt{\lambda_2} - \sqrt{\lambda_3} - \sqrt{\lambda_4} \right\}. \quad (5)$$

Concurrence satisfies  $0 \leq C(\rho) \leq 1$ , vanishing for separable states and achieving unity for maximally entangled two-qubit states. As an entanglement monotone, it is non-increasing under local operations and classical communication (LOCC).

*a) Relevance to ISDI-QKD.:* Concurrence provides a quantitative bridge between state quality and protocol security. However, a central finding of our work is that positive concurrence is *necessary but not sufficient* for secure key generation: the state must violate the relevant steering inequality by a sufficient margin, which requires entanglement exceeding a threshold that depends on noise type. Tracking

TABLE I: Summary of notation.

Symbol	Description
$r_\infty$	Asymptotic secure key rate (bits/pair)
$\eta_B$	Bob's detection efficiency
$H(A_1 B_1)$	Bob's uncertainty about Alice's outcomes
$H(A_1 E)$	Eve's uncertainty about Alice's outcomes
$C(\rho)$	Concurrence of state $\rho$
$p$	Dephasing probability
$\gamma$	Amplitude damping parameter
$q$	Depolarizing probability
$F$	Fidelity with target Bell state $ \Phi^+\rangle$
$L$	Fiber length (km)
$L_c$	Coherence length (km)

concurrence alongside key rates reveals where security fails despite residual entanglement, a phenomenon we term the “security-entanglement gap.”

For clarity, we summarize the key notation used throughout this paper in Table I.

## III. PROTOCOL AND NOISE MODELS

In this section, we describe the one-sided device-independent QKD protocol analyzed in this work. Our protocol builds upon the BBM92 entanglement-based scheme [18], the entanglement-based analog of BB84, adapted to the one-sided device-independent setting following Branciard *et al.* [9] and incorporating the recent efficiency improvements of Masini and Sarkar [11]. We detail the protocol assumptions, measurement procedures, security certification via steering inequalities, and the quantum noise models considered.

### A. Protocol Description

*1) The BBM92 Protocol and Its ISDI Adaptation:* The original BBM92 protocol [18], introduced by Bennett, Brassard, and Mermin in 1992, established that entanglement-based QKD could achieve equivalent security to prepare-and-measure BB84 [19] without requiring Bell inequality violation. Instead, BBM92 relies on the monogamy of entanglement: if Alice and Bob share a maximally entangled state, no third party (Eve) can be correlated with their measurement outcomes.

In standard BBM92, both parties possess trusted, well-characterized measurement devices. Our protocol modifies this assumption to achieve *one-sided device independence*:

- **Alice (trusted):** Possesses a fully characterized measurement device. Her detectors and measurement bases are assumed to operate as specified, as in standard BBM92.
- **Bob (untrusted):** His measurement device is treated as a black box. No assumptions are made about its internal workings; security must be certified from observed correlations alone.
- **Source:** An entangled photon source prepares two-qubit states and distributes one qubit to each party. We assume the source is located near Bob, so Alice's qubit traverses the noisy quantum channel.

This hybrid approach, combining the practical two-setting measurement structure of BBM92 with one-sided device independence, offers a middle ground between fully trusted QKD (vulnerable to detector attacks) and fully device-independent QKD (requiring impractically high detection efficiencies). Security certification shifts from device characterization to observable steering correlations.

2) *Trust Model Motivation:* The asymmetric trust model is natural in practical deployment scenarios:

- A bank or government server maintains well-characterized laboratory equipment with trusted detectors (Alice).
- A mobile client or remote user employs commodity hardware that may be compromised, poorly calibrated, or supplied by an untrusted vendor (Bob).

By removing trust assumptions on Bob's device, the protocol remains secure even if Bob's detectors are manipulated by an adversary, a significant advantage over standard BBM92.

3) *Initial State:* The entangled source prepares states of the form

$$|\psi(\theta)\rangle_{AB} = \cos \theta |00\rangle_{AB} + \sin \theta |11\rangle_{AB}, \quad (6)$$

where  $|0\rangle$  and  $|1\rangle$  denote computational basis states. The parameter  $\theta \in [0, \pi/2]$  controls the degree of entanglement:

- $\theta = 0$  or  $\pi/2$ : Separable product states (no entanglement)
- $\theta = \pi/4$ : Maximally entangled Bell state  $|\Phi^+\rangle = \frac{1}{\sqrt{2}}(|00\rangle + |11\rangle)$

Unless otherwise stated, we assume  $\theta = \pi/4$  for optimal baseline performance, consistent with standard BBM92 implementations. The complete protocol is provided in Table II

### B. Measurement Settings

Following the BBM92 structure, both parties measure in two mutually unbiased bases corresponding to the Pauli  $\sigma_z$  and  $\sigma_x$  observables.

1) *Alice's Measurements (Trusted):* Alice performs projective measurements in two bases:

$$\text{Setting } x = 1 : \quad \mathcal{M}_A^{(1)} = \{|0\rangle\langle 0|, |1\rangle\langle 1|\} \quad (\sigma_z \text{ basis}), \quad (7)$$

$$\text{Setting } x = 2 : \quad \mathcal{M}_A^{(2)} = \{|+\rangle\langle +|, |-\rangle\langle -|\} \quad (\sigma_x \text{ basis}), \quad (8)$$

TABLE II

Protocol 1: One-Sided Device-Independent BBM92	
<b>Setup:</b>	Alice and Bob share an authenticated classical channel and are connected by a quantum channel. An entangled source prepares $N$ copies of $ \psi(\theta)\rangle_{AB}$ .
<b>Quantum Phase:</b>	
1.	For each round $i \in \{1, \dots, N\}$ :
(a)	The source distributes one qubit to Alice and one to Bob (Alice's qubit traverses the noisy channel).
(b)	Alice randomly selects measurement setting $x_i \in \{1, 2\}$ and records outcome $a_i \in \{0, 1\}$ .
(c)	Bob randomly selects measurement setting $y_i \in \{1, 2\}$ and records outcome $b_i \in \{0, 1, \emptyset\}$ , where $\emptyset$ denotes no detection.
2.	Alice and Bob publicly announce their measurement settings $\{x_i\}$ and $\{y_i\}$ (but not outcomes).
<b>Parameter Estimation:</b>	
3.	From a randomly selected subset of rounds, Alice and Bob publicly compare outcomes to estimate: <ul style="list-style-type: none"> <li>• Joint probability distributions <math>p(a, b x, y)</math> for all settings</li> <li>• The steering parameter <math>S_2</math> (Eq. 12)</li> </ul>
4.	If $S_2 > 1/\sqrt{2}$ (steering inequality violated), proceed. Otherwise, abort the protocol.
<b>Key Distillation:</b>	
5.	Using remaining rounds where $(x_i, y_i) = (1, 1)$ and $b_i \neq \emptyset$ : <ul style="list-style-type: none"> <li>• Alice's outcomes <math>\{a_i\}</math> form her raw key</li> <li>• Bob's outcomes <math>\{b_i\}</math> form his raw key</li> </ul>
6.	Apply error correction to reconcile discrepancies.
7.	Apply privacy amplification to distill the final secure key.

where  $|\pm\rangle = \frac{1}{\sqrt{2}}(|0\rangle \pm |1\rangle)$ .

Since Alice's device is trusted, we apply the *fair-sampling assumption*: rounds where her detector fails to click are discarded. This is justified by her device characterization, which ensures non-detection events are random and uncorrelated with the quantum state.

2) *Bob's Measurements (Untrusted):* Bob's device is treated as a black box producing outcomes correlated with his input setting. Crucially, we *cannot* assume fair sampling on Bob's side, doing so would open the detection loophole, allowing an adversary to fake quantum correlations by selectively triggering or suppressing detection events.

To rigorously account for detector inefficiency, we model Bob's effective measurement as a three-outcome POVM. For detection efficiency  $\eta_B$  and nominal basis  $p \in \{z, x\}$ , let  $\Pi_{0|p}$  and  $\Pi_{1|p}$  be the ideal projectors satisfying  $\Pi_{0|p} + \Pi_{1|p} = \mathbb{I}$ . Bob's effective POVM elements are:

$$M_{0|p}^{(\eta)} = \eta_B \Pi_{0|p}, \quad M_{1|p}^{(\eta)} = \eta_B \Pi_{1|p}, \quad M_{\emptyset|p}^{(\eta)} = (1 - \eta_B) \mathbb{I}. \quad (9)$$

Completeness is readily verified:  $M_{0|p}^{(\eta)} + M_{1|p}^{(\eta)} + M_{\emptyset|p}^{(\eta)} = \mathbb{I}$ .

The no-detection outcome  $\emptyset$  is explicitly included in all statistical analyses. This conservative treatment is essential for device-independent security: by accounting for all possible outcomes, we prevent an adversary from exploiting detection inefficiency to compromise the protocol.

### C. Security via Steering Inequality

Unlike standard BBM92, which derives security from trusted device operation, our 1SDI adaptation certifies security through the violation of a *steering inequality*, an observable

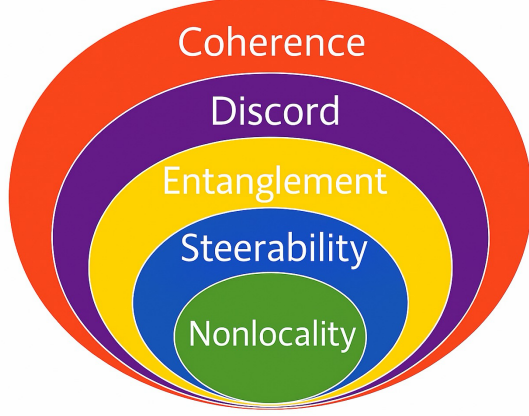


Fig. 2: Hierarchy of quantum correlations. Nested sets illustrate the strict inclusion relations among different classes of quantum correlations: coherence (outermost)  $\supset$  discord  $\supset$  entanglement  $\supset$  steerability  $\supset$  nonlocality (innermost). States exhibiting nonlocality form the most restrictive class, while coherence represents the broadest quantum feature. One-sided device-independent QKD exploits steerability, a strictly intermediate resource between entanglement and nonlocality, enabling security certification without requiring full Bell inequality violation or complete device trust [20].

test that cannot be passed by any local hidden state model. As shown in Fig. 2, quantum correlations form a strict hierarchy:

$$\begin{aligned} \text{Nonlocality} &\subset \text{Steerability} \subset \text{Entanglement} \subset \\ &\subset \text{Discord} \subset \text{Coherence}. \end{aligned} \quad (10)$$

While fully device-independent QKD requires nonlocality (Bell violation), the 1SDI framework operates at the steerability level, a weaker but more noise-robust requirement. This positions our protocol advantageously: it tolerates higher channel noise than DI-QKD while providing stronger security guarantees than standard entanglement-based schemes that assume trusted devices.

1) *Quantum Steering as Security Certificate*: Quantum steering [21] is an asymmetric form of quantum nonlocality, intermediate between entanglement and Bell nonlocality. In a steering scenario, Alice (the trusted party) can verify that Bob's system is genuinely entangled with hers by demonstrating that the conditional states she can "steer" Bob's system into cannot be explained by any *local hidden state* (LHS) model.

Branciard *et al.* [9] established that steering is both *necessary* and *sufficient* for secure 1SDI-QKD:

- **Necessary:** If the observed correlations admit an LHS model (no steering), then Eve could possess a copy of Bob's local hidden state, making secure key generation impossible.
- **Sufficient:** If steering is demonstrated, the correlations cannot be explained without genuine entanglement between Alice and Bob, guaranteeing that Eve's information is bounded.

2) *The Two-Setting Linear Steering Inequality*: For our BBM92-based protocol with two measurement settings per party, the relevant steering inequality is [22]:

$$S_2 = \frac{1}{2} |\langle A_1 B_1 \rangle + \langle A_2 B_2 \rangle| \leq C_2^{\text{LHS}}, \quad (11)$$

where  $A_k$  and  $B_k$  denote Alice's and Bob's measurement observables for setting  $k$ , and  $C_2^{\text{LHS}}$  is the maximum value achievable by any LHS model.

With our specific choice of measurements ( $A_1 = B_1 = \sigma_z$  and  $A_2 = B_2 = \sigma_x$ ), the steering parameter becomes:

$$S_2 = \frac{1}{2} (\langle \sigma_z \otimes \sigma_z \rangle + \langle \sigma_x \otimes \sigma_x \rangle), \quad (12)$$

with the LHS bound:

$$S_2 \leq \frac{1}{\sqrt{2}} \approx 0.707. \quad (13)$$

For the maximally entangled state  $|\Phi^+\rangle$  with ideal measurements and detection,  $\langle \sigma_z \otimes \sigma_z \rangle = \langle \sigma_x \otimes \sigma_x \rangle = 1$ , yielding  $S_2 = 1$ , a maximal violation of the steering inequality. Noise and detection inefficiency reduce this value; the protocol remains secure only while  $S_2 > 1/\sqrt{2}$ .

3) *From Steering Violation to Key Rate*: The observed steering parameter directly constrains Eve's information about Alice's measurement outcomes. Following the analysis of Masini and Sarkar [11], the conditional entropy  $H(A_1|E)$  appearing in the key rate formula (Eq. 1) is lower-bounded by a function of  $S_2$  and the detection statistics:

$$H(A_1|E) \geq f(S_2, \eta_B, \{p(a, b|x, y)\}), \quad (14)$$

where the function  $f$  is evaluated numerically using the BFF method [15] (see Section III-E).

The key intuition is:

- Higher steering violations  $\Rightarrow$  stronger quantum correlations  $\Rightarrow$  larger  $H(A_1|E)$   $\Rightarrow$  higher key rates.
- When  $S_2$  falls below  $1/\sqrt{2}$  due to noise, the correlations become classically explicable,  $H(A_1|E)$  can no longer be guaranteed sufficient, and secure key generation becomes impossible.

#### D. Quantum Noise Models

In realistic fiber-optic or free-space implementations, the quantum channel introduces noise that degrades entanglement and reduces steering correlations. We model three prevalent noise types using the Kraus operator formalism [23]. Unless stated otherwise, noise acts on Alice's qubit (which traverses the channel) via the map  $\rho'_{AB} = (\mathcal{E} \otimes \mathcal{I})(\rho_{AB})$ . We model one-sided channel noise on the traveling subsystem; for symmetric sources this choice is equivalent up to relabeling the parties, and we apply  $\mathcal{E}$  on Alice for notational convenience.

1) *Dephasing Channel*: Dephasing randomizes the relative phase between  $|0\rangle$  and  $|1\rangle$  without affecting state populations. It models:

- Phase noise from fluctuating optical path lengths [24]
- Magnetic field variations in atomic systems
- Timing jitter in photon detection

The Kraus operators are:

$$K_0 = \sqrt{1-p} \mathbb{I}, \quad K_1 = \sqrt{p} \sigma_z, \quad (15)$$

yielding the channel

$$\mathcal{E}_{\text{deph}}(\rho) = (1-p)\rho + p \sigma_z \rho \sigma_z. \quad (16)$$

In the computational basis, this damps off-diagonal elements by factor  $(1-2p)$ :

$$\rho = \begin{pmatrix} \rho_{00} & \rho_{01} \\ \rho_{10} & \rho_{11} \end{pmatrix} \xrightarrow{\mathcal{E}_{\text{deph}}} \begin{pmatrix} \rho_{00} & (1-2p)\rho_{01} \\ (1-2p)\rho_{10} & \rho_{11} \end{pmatrix}. \quad (17)$$

The dephasing probability relates to fiber length  $L$  via [25]:

$$p(L) = \frac{1}{2} \left( 1 - e^{-L/L_c} \right), \quad (18)$$

where  $L_c$  is the coherence length characterizing the channel's phase stability. Note that  $p \in [0, 0.5]$ ; at  $p = 0.5$ , complete dephasing occurs.

2) *Depolarizing Channel*: Depolarizing noise applies random Pauli errors with equal probability, uniformly shrinking the Bloch vector toward the maximally mixed state. It models:

- Isotropic environmental coupling
- Polarization mode dispersion in fibers
- Multiple weak noise sources acting together

The Kraus operators are:

$$\begin{aligned} K_0 &= \sqrt{1 - \frac{3q}{4}} \mathbb{I}, & K_1 &= \sqrt{\frac{q}{4}} \sigma_x, \\ K_2 &= \sqrt{\frac{q}{4}} \sigma_y, & K_3 &= \sqrt{\frac{q}{4}} \sigma_z, \end{aligned} \quad (19)$$

producing the channel

$$\mathcal{E}_{\text{depol}}(\rho) = (1-q)\rho + q \frac{\mathbb{I}}{2}. \quad (20)$$

This can be interpreted as: with probability  $(1-q)$  the state is transmitted perfectly; with probability  $q$  it is replaced by the maximally mixed state  $\mathbb{I}/2$ . The depolarizing probability varies with distance as:

$$q(L) = 1 - e^{-L/L_c}. \quad (21)$$

3) *Amplitude Damping Channel*: Amplitude damping models energy relaxation processes where excited states decay to ground states. It describes:

- Spontaneous emission in atomic systems
- Photon loss to the environment
- $T_1$  relaxation in superconducting qubits

The Kraus operators are:

$$K_0 = \begin{pmatrix} 1 & 0 \\ 0 & \sqrt{1-\gamma} \end{pmatrix}, \quad K_1 = \begin{pmatrix} 0 & \sqrt{\gamma} \\ 0 & 0 \end{pmatrix}, \quad (22)$$

yielding the transformation

$$\mathcal{E}_{\text{ad}}(\rho) = \begin{pmatrix} \rho_{00} + \gamma \rho_{11} & \sqrt{1-\gamma} \rho_{01} \\ \sqrt{1-\gamma} \rho_{10} & (1-\gamma) \rho_{11} \end{pmatrix}. \quad (23)$$

Unlike dephasing and depolarizing channels, amplitude damping is *asymmetric*: it favors  $|0\rangle$  over  $|1\rangle$ , breaking

TABLE III: Summary of quantum noise channels studied in this work.

Channel	Parameter	Range	Physical Origin
Dephasing	$p$	$[0, 0.5]$	Phase fluctuations
Depolarizing	$q$	$[0, 1]$	Isotropic noise
Amplitude damping	$\gamma$	$[0, 1]$	Energy relaxation

the symmetry of Bell-diagonal states. This has important consequences for entanglement purification, as discussed in Section V.

The damping parameter scales with distance as:

$$\gamma(L) = 1 - e^{-L/L_c}. \quad (24)$$

Table III summarizes the three noise channels and their characteristics.

In practice, multiple noise sources may act simultaneously. However, to isolate their individual impacts on 1SDI-QKD performance, we analyze each channel separately in Section IV. Combined noise scenarios can be treated by composing the respective channels.

#### E. Simulation Methodology

To evaluate secure key rates under noise, we implement the following numerical procedure:

- 1) **State preparation:** Initialize the two-qubit state  $\rho_0 = |\psi(\theta)\rangle\langle\psi(\theta)|$  with  $\theta = \pi/4$  (maximally entangled) unless otherwise specified.
- 2) **Noise application:** Apply the relevant noise channel to Alice's qubit:

$$\rho_{AB} = (\mathcal{E} \otimes \mathcal{I})(\rho_0). \quad (25)$$

- 3) **Measurement statistics:** Compute joint probability distributions

$$p(a, b|x, y) = \text{Tr} \left[ \left( M_a^{(x)} \otimes M_b^{(y, \eta_B)} \right) \rho_{AB} \right] \quad (26)$$

for all measurement setting combinations  $(x, y) \in \{1, 2\}^2$  and outcomes  $(a, b)$ , incorporating Bob's detection efficiency via Eq. (9).

- 4) **Steering parameter:** Calculate  $S_2$  from the observed correlations using Eq. (12).
- 5) **Entropy estimation:**

- $H(A_1|B_1)$ : Computed directly from  $p(a, b|1, 1)$  using Eq. (2).
- $H(A_1|E)$ : Lower-bounded using the Brown-Fawzi-Fawzi (BFF) method [15] with NPA hierarchy level 2, implemented via the NCPOL2SDPA package [26] with the MOSEK solver [27].

- 6) **Key rate:** Compute the asymptotic secure key rate:

$$r_\infty = H(A_1|E) - H(A_1|B_1). \quad (27)$$

- 7) **Entanglement quantification:** Calculate the concurrence  $C(\rho_{AB})$  using Eq. (5) to track entanglement degradation.

TABLE IV: Critical noise thresholds for 1SDI-QKD security. The key rate threshold  $p_{\text{crit}}^{(r)}$  indicates where  $r \rightarrow 0$  at  $\eta_B = 1$ . The steering threshold  $p_{\text{crit}}^{(S)}$  indicates where  $S_2$  reaches the classical bound. The gap between these thresholds reflects the additional penalty from increased  $H(A_1|B_1)$ .

Noise Type	$p_{\text{crit}}^{(r)}$	$p_{\text{crit}}^{(S)}$	$\eta_B^{\min}$ at $p = 0.1$	Tolerance
Dephasing	$\approx 0.50$	0.50	$\sim 55\%$	High
Amplitude damping	$\approx 0.36$	0.42	$\sim 85\%$	Low
Depolarizing	$\approx 0.24$	0.29	$\sim 90\%$	Very low

**Numerical parameters:** All simulations use 100 efficiency values uniformly spaced in  $\eta_B \in [0.4, 1.0]$  and noise parameters sampled at intervals of 0.01 for threshold determination. For distance-dependent analyses in Section V, we employ noise-type-specific coherence lengths that reflect the distinct physical origins of each decoherence mechanism (see Section V for details).

#### IV. RESULTS

We present simulation results characterizing 1SDI-QKD performance under realistic noise conditions. We first validate our numerical framework against known theoretical limits, then systematically analyze the impact of each noise type on secure key rates, detection efficiency requirements, and entanglement degradation.

##### A. Validation of Numerical Framework

Before analyzing noise effects, we validated our implementation by reproducing the fundamental efficiency threshold for 1SDI-QKD. In the absence of noise ( $p = 0$ ), our simulations yield a minimum detection efficiency of  $\eta_B^{\min} \approx 50.1\%$  for positive key generation, consistent with the theoretical prediction of Masini and Sarkar [11]. This threshold approaches the fundamental limit for any two-setting steering-based protocol, confirming the correctness of our BFF/NPA implementation.

##### B. Impact of Quantum Noise on Secure Key Rates

We investigate how each noise type affects the secure key rate  $r$  of the 1SDI-QKD protocol. Unless stated otherwise, the initial shared state is maximally entangled ( $\theta = \pi/4$ ), providing the highest baseline key rate.

1) *Key Rate versus Detection Efficiency:* Figures 3a, 3b, 3c show the secure key rate as a function of Bob's detection efficiency  $\eta_B$  for varying noise levels. The three noise types exhibit markedly different behaviors:

a) *Dephasing noise:* Dephasing has a comparatively mild impact on efficiency requirements. Even at  $p = 0.3$  (30% dephasing probability), positive key rates remain achievable with  $\eta_B \approx 70\%$ . This tolerance arises because dephasing preserves the diagonal (population) elements of the density matrix while only degrading coherences. Since the  $\sigma_z$  measurement used for key generation is insensitive to phase, dephasing affects security primarily through reduced  $\sigma_x$  correlations needed for steering verification.

The efficiency threshold  $\eta_B^{\min}(p)$  under dephasing can be approximated by:

$$\eta_B^{\min}(p) \approx \frac{\eta_0}{1 - 2p + 2p^2}, \quad (28)$$

where  $\eta_0 \approx 0.501$  is the noise-free threshold. This approximation, derived from the steering parameter degradation, agrees with numerical results to within 3% for  $p \leq 0.3$ .

b) *Amplitude damping:* Amplitude damping dramatically elevates efficiency requirements. A damping probability of  $\gamma = 0.1$  increases the threshold to  $\eta_B^{\min} \approx 85\%$ , and  $\gamma \geq 0.2$  demands near-unity detection efficiency. This severe impact reflects amplitude damping's dual degradation mechanism: it reduces both populations (through decay  $|1\rangle \rightarrow |0\rangle$ ) and coherences (through the  $\sqrt{1-\gamma}$  damping factor), simultaneously weakening correlations in both measurement bases.

c) *Depolarizing noise:* Depolarizing noise exhibits behavior similar to amplitude damping, with efficiency requirements sharply approaching 100% as  $q$  increases. At  $q = 0.2$  (20% depolarization), near-perfect detection is required for any positive key rate. Depolarizing noise uniformly contracts the Bloch vector, reducing steering correlations in all directions equally, leaving minimal margin for additional losses from imperfect detection.

2) *Key Rate versus Noise Strength:* To isolate the effect of noise from detection inefficiency, Fig. 4 plots the secure key rate as a function of noise parameter for each channel at ideal detection efficiency ( $\eta_B = 1$ ). This reveals the intrinsic noise tolerance of the protocol:

a) *Critical noise thresholds:* Each noise type exhibits a critical threshold beyond which no secure key can be extracted:

- **Amplitude damping:**  $\gamma_{\text{crit}} \approx 0.36$
- **Depolarizing:**  $q_{\text{crit}} \approx 0.24$
- **Dephasing:**  $p_{\text{crit}} \approx 0.50$

The ordering  $q_{\text{crit}} < \gamma_{\text{crit}} < p_{\text{crit}}$  establishes a clear *noise hierarchy*: depolarizing noise is most detrimental, followed by amplitude damping, with dephasing being most tolerable.

These thresholds can be understood through the steering parameter  $S_2$ . For a maximally entangled initial state subjected to one-sided noise, the steering parameter evaluates to:

$$S_2^{\text{deph}}(p) = \frac{1}{2}(1 + |1 - 2p|), \quad (29)$$

$$S_2^{\text{depol}}(q) = 1 - q, \quad (30)$$

$$S_2^{\text{ad}}(\gamma) = \frac{1}{2}(1 - \gamma + \sqrt{1 - \gamma}). \quad (31)$$

Security requires  $S_2 > 1/\sqrt{2} \approx 0.707$ . Solving for the critical noise values:

$$p_{\text{crit}}^{\text{steering}} = \frac{1}{2}\left(1 - \frac{1}{\sqrt{2}}\right) \approx 0.146, \quad (32)$$

$$q_{\text{crit}}^{\text{steering}} = 1 - \frac{1}{\sqrt{2}} \approx 0.293, \quad (33)$$

$$\gamma_{\text{crit}}^{\text{steering}} \approx 0.42. \quad (34)$$

The numerically observed thresholds ( $\gamma_{\text{crit}} \approx 0.36$ ,  $q_{\text{crit}} \approx 0.24$ ) are *lower* than these steering-based estimates because

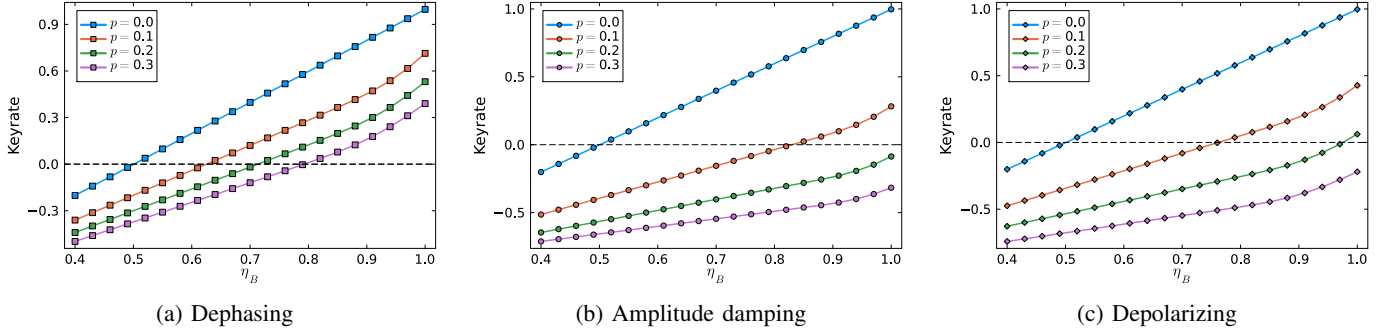


Fig. 3: Secure key rate  $r$  versus Bob's detection efficiency  $\eta_B$  under different noise models with noise probabilities  $p = 0.0$  (blue),  $0.1$  (orange),  $0.2$  (green), and  $0.3$  (purple). (a) Dephasing noise induces a gradual elevation of the minimum efficiency threshold, maintaining positive key rates at  $\eta_B \approx 0.65$  even for  $p = 0.3$ . (b) Amplitude damping sharply elevates efficiency requirements; at  $p = 0.3$ , detection efficiencies exceeding  $90\%$  are necessary. (c) Depolarizing noise exhibits similar behavior to amplitude damping, with the most stringent efficiency thresholds among all noise models.

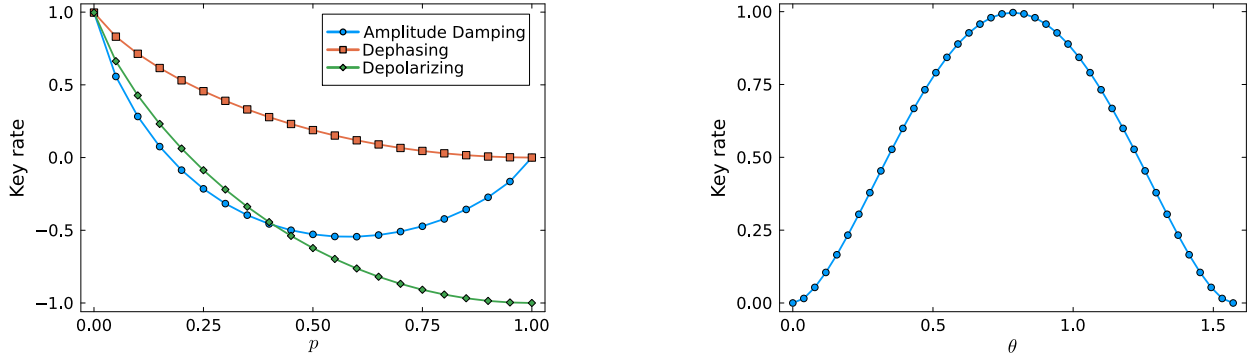


Fig. 4: Secure key rate  $r$  as a function of noise strength for amplitude damping (blue circles), dephasing (orange squares), and depolarizing (green diamonds) channels at ideal detection efficiency  $\eta_B = 1$ . Vertical dashed lines indicate critical thresholds where  $r \rightarrow 0$ .

the key rate depends on both  $H(A_1|E)$  and  $H(A_1|B_1)$ . Noise increases Bob's uncertainty  $H(A_1|B_1)$ , causing key rates to vanish before the steering inequality is actually violated.

Table IV summarizes the critical thresholds and their practical implications. The clear noise hierarchy suggests prioritized mitigation strategies:

- 1) **Depolarizing noise** (most harmful): Requires active polarization tracking and stabilization. Consider time-bin or phase encoding to avoid polarization-dependent errors.
- 2) **Amplitude damping** (severe): Minimize transmission loss through high-quality optics. Position the entangled source closer to Alice (the lossy channel side) rather than Bob.
- 3) **Dephasing** (most tolerable): Standard interferometric stabilization suffices. Focus engineering efforts on the more damaging noise sources.

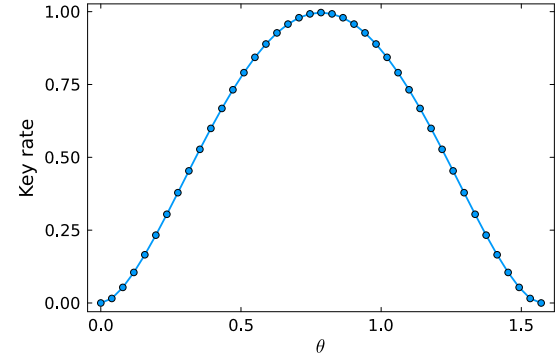


Fig. 5: Secure key rate  $r$  versus entanglement angle  $\theta$  of the initial state  $|\psi(\theta)\rangle$ , assuming ideal detection efficiency ( $\eta_B = 1$ ) and no channel noise. The maximum occurs at  $\theta = \pi/4$  (maximally entangled state), with key rates vanishing as the state becomes separable.

### C. Impact of Initial Entanglement

We next examine how the initial entanglement level affects protocol performance. Figure 5 shows the secure key rate versus the entanglement parameter  $\theta$  for an ideal detector and no channel noise.

1) *Optimal Entanglement*: The maximum key rate occurs at  $\theta = \pi/4$  (the maximally entangled Bell state  $|\Phi^+\rangle$ ), as expected from theoretical considerations. The key rate drops symmetrically as  $\theta$  deviates from  $\pi/4$  in either direction, vanishing at  $\theta = 0$  and  $\theta = \pi/2$  (separable states).

The dependence can be understood analytically. For the state  $|\psi(\theta)\rangle = \cos \theta |00\rangle + \sin \theta |11\rangle$ , the steering parameter evaluates to:

$$S_2(\theta) = \frac{1}{2}(1 + \sin 2\theta), \quad (35)$$

which achieves its maximum of 1 at  $\theta = \pi/4$  and falls below the classical bound  $1/\sqrt{2}$  for  $\theta < \theta_{\min}$  or  $\theta > \pi/2 - \theta_{\min}$ ,

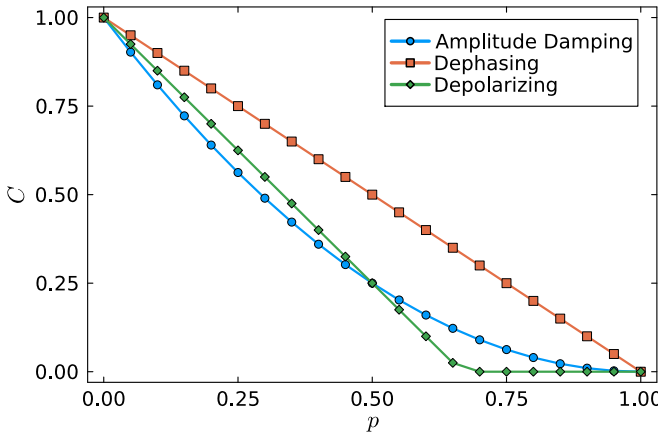


Fig. 6: Concurrence  $C$  versus noise parameter for amplitude damping (blue), depolarizing (green), and dephasing (orange) channels applied to one qubit of an initially maximally entangled state. Markers indicate entanglement sudden death (ESD) points where  $C \rightarrow 0$ . Dashed vertical lines show the corresponding key rate thresholds from Table IV.

where:

$$\theta_{\min} = \frac{1}{2} \arcsin(\sqrt{2} - 1) \approx 0.304 \text{ rad} \approx 17.4^\circ. \quad (36)$$

2) *Entanglement and Noise Interplay*: Under noise, highly entangled initial states generally outperform weakly entangled ones, they provide a larger “buffer” against noise-induced degradation. A weakly entangled source ( $\theta$  near 0.2 rad, concurrence  $C \approx 0.38$ ) may lose all entanglement under moderate noise, while a maximally entangled source retains sufficient correlations for key generation.

However, we observed a subtle effect with amplitude damping: because this channel preferentially decays the  $|11\rangle$  component, states with  $\theta > \pi/4$  (biased toward  $|11\rangle$ ) suffer greater degradation than those with  $\theta < \pi/4$ . This asymmetry suggests that in amplitude-damping-dominated channels, slightly  $|00\rangle$ -biased states ( $\theta$  slightly below  $\pi/4$ ) might offer marginal advantages, though the effect is small in our simulations.

#### D. Entanglement Degradation and the Security-Entanglement Gap

A central finding of this work is that secure key generation fails *before* entanglement vanishes, a phenomenon we term the “security-entanglement gap.” Understanding this gap is crucial for assessing when purification or other countermeasures are necessary.

1) *Concurrence under Noise*: Figure 6 shows the concurrence  $C$  as a function of noise parameter for each channel, with noise applied to one qubit of an initially maximally entangled state. The three channels exhibit qualitatively different entanglement dynamics:

a) *Amplitude damping*: Concurrence decreases continuously as:

$$C(\gamma) = \sqrt{1 - \gamma}, \quad (37)$$

TABLE V: Comparison of security and entanglement thresholds, demonstrating the security-entanglement gap. The residual concurrence  $C$  at the key-rate threshold quantifies remaining entanglement when security is lost.

Noise Type	$p_{\text{crit}} (r \rightarrow 0)$	$p_{\text{ESD}} (C \rightarrow 0)$	$C$ at $p_{\text{crit}}$
Dephasing	$\approx 0.50$	0.50	$\sim 0$
Amplitude damping	$\approx 0.36$	1.00	$\approx 0.80$
Depolarizing	$\approx 0.24$	0.67	$\approx 0.64$

approaching zero only at complete damping ( $\gamma = 1$ ). Notably, *no entanglement sudden death occurs*, the decay is smooth and monotonic.

b) *Depolarizing noise*:: Concurrence decreases linearly until reaching zero at the entanglement sudden death (ESD) point:

$$C(q) = \max \left\{ 0, 1 - \frac{3q}{2} \right\}, \quad (38)$$

yielding  $q_{\text{ESD}} = 2/3 \approx 0.67$ . Beyond this point, the state is separable.

c) *Dephasing noise*: Concurrence exhibits non-monotonic behavior:

$$C(p) = |1 - 2p|, \quad (39)$$

reaching zero at  $p_{\text{ESD}} = 0.5$ , then *reviving* for  $p > 0.5$  as the state transforms toward  $|\Phi^-\rangle$ . At  $p = 1$  (complete phase flip),  $C = 1$  again. For practical purposes, the relevant regime is  $p < 0.5$ .

2) *The Security-Entanglement Gap*: Table V compares the key rate thresholds with the entanglement thresholds, revealing significant gaps:

a) *Key insight*:: For amplitude damping and depolarizing noise, the key rate vanishes while substantial entanglement remains ( $C \approx 0.64$ – $0.80$ ). This demonstrates that *entanglement is necessary but not sufficient for 1SDI-QKD security*. The protocol requires not merely nonzero entanglement, but sufficient entanglement to:

- 1) Violate the steering inequality ( $S_2 > 1/\sqrt{2}$ ), and
- 2) Maintain  $H(A_1|E) > H(A_1|B_1)$  despite noise-induced correlation degradation.

The only exception is dephasing, where security and entanglement thresholds coincide at  $p = 0.5$ . This occurs because dephasing affects only off-diagonal elements, and both steering violation and entanglement depend on the same coherence terms.

3) *Implications for Protocol Design*: The security-entanglement gap has important practical implications:

- 1) **Entanglement witnesses are insufficient**: Simply verifying that a shared state is entangled does not guarantee secure key generation. Steering-based certification is essential.
- 2) **Purification timing**: Entanglement purification should be initiated when key rates approach zero, not when entanglement approaches zero. Waiting until ESD wastes resources on states that cannot yield secure keys.

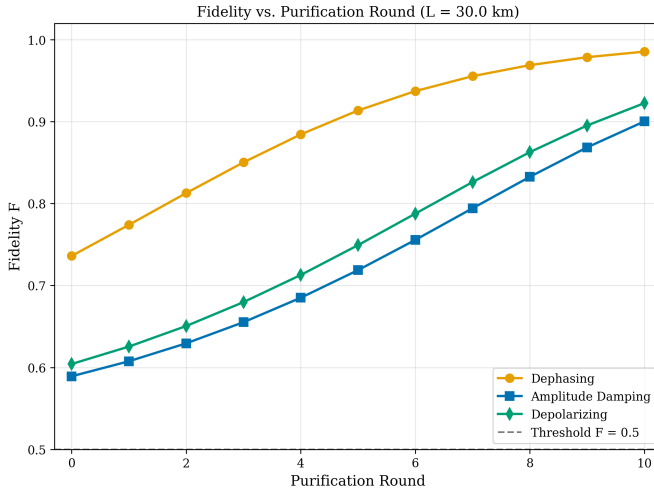


Fig. 7: Fidelity versus purification round for dephasing ( $L_c = 40$  km), amplitude damping ( $L_c = 24$  km), and depolarizing ( $L_c = 40$  km) noise at  $L = 30$  km. The dashed line indicates the purification threshold  $F = 0.5$ .

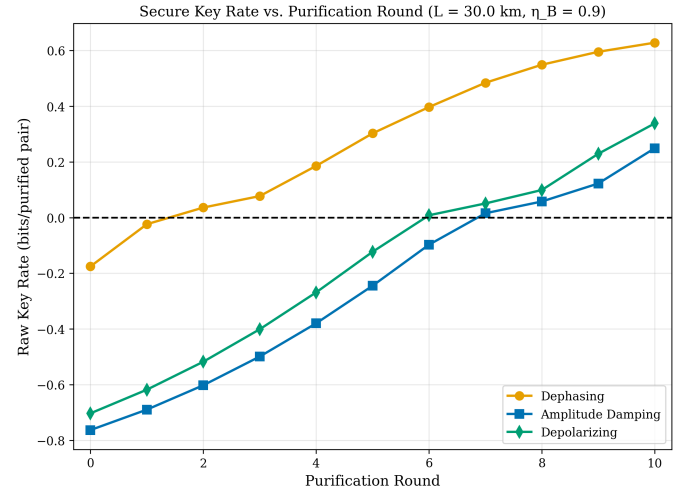


Fig. 8: Secure key rate versus purification round at  $L = 30$  km with  $\eta_B = 0.9$ . Purification enables positive key rates in regimes where unpurified states yield no secure key.

3) **Resource allocation:** The residual entanglement at  $p_{\text{crit}}$  ( $C \approx 0.64\text{--}0.80$ ) indicates that purification protocols, which typically require  $F > 0.5$  (equivalently  $C > 0$ ), remain viable even at the security threshold.

#### E. Numerical Precision and Reproducibility

All results presented in this section were obtained using:

- BFF entropy bounds computed at NPA hierarchy level 2
- MOSEK solver with default tolerance ( $10^{-8}$ )
- 100 uniformly spaced efficiency values in  $\eta_B \in [0.4, 1.0]$
- Noise parameters sampled at intervals of 0.01 for threshold determination

The reported threshold values ( $\gamma_{\text{crit}} \approx 0.36$ ,  $q_{\text{crit}} \approx 0.24$ ) have numerical uncertainty of approximately  $\pm 0.01$ , limited by the noise parameter sampling resolution. Convergence was verified by comparing NPA levels 1 and 2; level-2 results were consistently tighter by 2–5% but thresholds remained stable.

## V. ENTANGLEMENT PURIFICATION FOR NOISE MITIGATION

Having established that realistic noise substantially impairs 1SDI-QKD performance, often eliminating secure key generation entirely, we investigate entanglement purification as a countermeasure. Purification protocols distill high-fidelity entangled pairs from larger ensembles of noisy pairs, potentially restoring the correlations needed for secure key generation.

#### A. The BBPSSW Purification Protocol

We employ the BBPSSW protocol [12], which operates on pairs of noisy entangled states to probabilistically produce a single higher-fidelity pair. The protocol proceeds as follows: (1) Alice and Bob each apply a CNOT gate between their respective qubits from two shared pairs, (2) both measure their target qubits in the computational basis, (3) they compare

outcomes via classical communication, and (4) if outcomes agree, the control pair is kept with improved fidelity; otherwise both pairs are discarded.

For input states in Werner form, the output fidelity after one successful round is [12]:

$$F' = \frac{F^2 + \frac{1}{9}(1-F)^2}{F^2 + \frac{2}{3}F(1-F) + \frac{5}{9}(1-F)^2}. \quad (40)$$

This recurrence has a stable fixed point at  $F = 1$  and an unstable fixed point at  $F = 1/2$ . Consequently, for  $F > 1/2$ , repeated purification drives  $F \rightarrow 1$ , while for  $F < 1/2$ , purification fails.

The success probability for each round is:

$$P_{\text{succ}}(F) = F^2 + \frac{2}{3}F(1-F) + \frac{5}{9}(1-F)^2. \quad (41)$$

#### B. Pauli Twirling for Non-Bell-Diagonal States

The BBPSSW protocol assumes Bell-diagonal input states. However, amplitude damping produces non-Bell-diagonal states. Although twirling preserves the Bell-state fidelity, it can reduce other entanglement and correlation measures. Therefore, in our security analysis we compute the secret key rate from the measurement statistics of the twirled (Bell-diagonal) state used as input to purification. Before purification, such states must be converted to Bell-diagonal form via Pauli twirling:

$$\mathcal{T}(\rho) = \frac{1}{4} \sum_{i \in \{I, X, Y, Z\}} (\sigma_i \otimes \sigma_i) \rho (\sigma_i \otimes \sigma_i). \quad (42)$$

Twirling preserves fidelity but reduces concurrence for non-Bell-diagonal states. For amplitude damping at noise parameter  $p = 0.3$ , twirling reduces concurrence by approximately 18% (from  $C = 0.837$  to  $C = 0.687$ ) while maintaining  $F = 0.843$ .

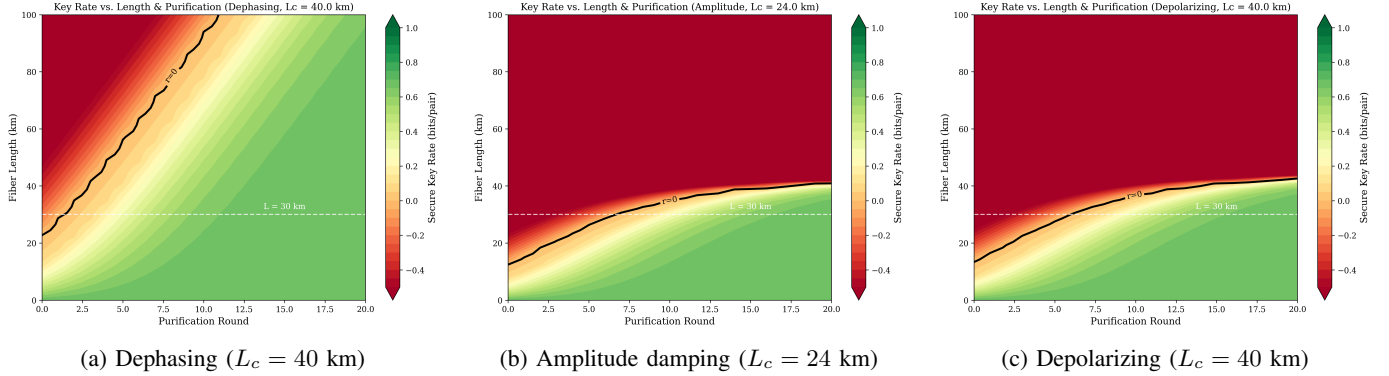


Fig. 9: Secure key rate versus fiber length and purification round. The zero-contour (black line) separates operational and non-operational regimes. The white dashed line marks  $L = 30$  km.

TABLE VI: Implied noise strengths at  $L = 30$  km using the distance-dependent models.

Noise type	$L_c$ (km)	Noise parameter at $L = 30$ km
Dephasing	40	$p = \frac{1}{2}(1 - e^{-30/40}) \approx 0.264$
Amplitude damping	24	$\gamma = 1 - e^{-30/24} \approx 0.713$
Depolarizing	40	$q = 1 - e^{-30/40} \approx 0.528$

### C. Purification Results

We present results for BBPSSW purification at fiber length  $L = 30$  km. To model the distinct physical mechanisms underlying each noise type, we employ noise-type-specific coherence lengths:  $L_c = 40$  km for dephasing,  $L_c = 24$  km for amplitude damping, and  $L_c = 40$  km for depolarizing noise [28].

1) *Fidelity Improvement*: Figure 7 shows the fidelity evolution over purification rounds. All noise types satisfy  $F > 0.5$  at  $L = 30$  km, ensuring purification convergence. Dephasing starts at  $F \approx 0.74$  and reaches  $F > 0.95$  within 3–4 rounds. Amplitude damping and depolarizing start at  $F \approx 0.58$ –0.60 and achieve  $F > 0.90$  after 5–6 rounds.

2) *Secure Key Rate Enhancement*: Figure 8 shows the secure key rate versus purification round. The critical observation is that purification converts *impossible* key generation ( $r \leq 0$ ) to *possible* ( $r > 0$ ). For amplitude damping and depolarizing, initial key rates are negative, but after 2–3 purification rounds, positive key rates emerge.

### D. Operating Regime Maps

Figure 9 presents contour plots of secure key rate as a function of fiber length and purification round. The zero-contour (black line) separates regions where positive key generation is possible from those where it is not. Dephasing permits the largest secure region, while depolarizing restricts operation to shorter distances. Beyond approximately ten rounds, expansion of the secure region saturates.

Table VII summarizes operational guidelines. The BBPSSW protocol consumes  $2^n$  initial pairs per output pair after  $n$  rounds; for the parameters studied, 2–4 rounds provide the

TABLE VII: Recommended purification strategy by operating regime.

Regime	Rounds	Rationale
Short ( $L < 15$ km)	0	Initial rates already positive
Medium (15–35 km)	2–4	Restores security
Long ( $L > 35$ km)	> 5	Consider quantum repeaters

best balance between fidelity improvement and resource consumption.

## VI. CONCLUSION

We have presented the first comprehensive noise analysis of one-sided device-independent QKD, extending the 1SDI-QKD framework of Masini and Sarkar [11] to realistic quantum channels. Our work addresses a critical gap between theoretical security proofs, which assume idealized conditions, and the practical deployment of 1SDI-QKD over noisy fiber-optic networks.

Our analysis establishes a clear noise hierarchy: dephasing is most tolerable, permitting secure key generation at 70% detection efficiency with 30% noise, while amplitude damping and depolarizing errors demand near-unity efficiency for comparable noise levels. A key finding is that secure key rates vanish while substantial entanglement persists ( $C \approx 0.68$ –0.80 at the security threshold), demonstrating that 1SDI-QKD requires sufficient steering inequality violation, not merely nonzero entanglement. This distinction has direct implications for system design: optimizing entanglement alone is insufficient without ensuring adequate steering correlations.

The BBPSSW entanglement purification protocol proves effective at restoring security in otherwise insecure regimes. However, our resource overhead analysis reveals that effective key rates peak at 2–4 purification rounds due to exponential pair consumption ( $2^n$ ), beyond which further purification becomes counterproductive. This establishes metropolitan-scale distances (15–35 km) as the optimal operating regime where purification provides meaningful benefit without prohibitive resource costs.

Situated between the stringent requirements of fully DI-QKD (which demands >82% efficiency and loophole-free Bell

tests) and the partial trust assumptions of MDI-QKD (which requires trusted state preparation), 1SDI-QKD offers a pragmatic intermediate: true device independence on the untrusted side with substantially relaxed efficiency requirements. Our results confirm that this advantage persists under realistic noise when combined with appropriate purification strategies.

Several directions warrant future investigation: (i) finite-key security analysis for practical block sizes, where statistical fluctuations may further constrain operating regimes [29]; (ii) experimental validation using state-of-the-art photon sources and superconducting nanowire detectors [30]; (iii) alternative purification protocols such as DEJMPS [31] or hashing-based schemes that may offer improved resource efficiency; and (iv) integration with quantum repeater architectures for range extension beyond metropolitan scales [32].

These findings establish quantitative boundaries for practical 1SDI-QKD deployment and demonstrate that noise-aware entanglement management provides a viable path from theoretical security to real-world quantum key distribution.

## REFERENCES

- [1] P. W. Shor, "Algorithms for quantum computation: discrete logarithms and factoring," in *Proceedings 35th annual symposium on foundations of computer science*, pp. 124–134, Ieee, 1994.
- [2] V. Scarani, H. Bechmann-Pasquinucci, N. J. Cerf, M. Dušek, N. Lütkenhaus, and M. Peev, "The security of practical quantum key distribution," *Reviews of modern physics*, vol. 81, no. 3, pp. 1301–1350, 2009.
- [3] C. BENNET, "Quantum cryptography: Public key distribution and coin tossing," in *Proceedings of the IEEE International Conference on Computers, Systems, and Signal Processing, Bangalore, Dec. 1984*, pp. 175–179, 1984.
- [4] I. Gerhardt, Q. Liu, A. Lamas-Linares, J. Skaar, C. Kurtsiefer, and V. Makarov, "Full-field implementation of a perfect eavesdropper on a quantum cryptography system," *Nature communications*, vol. 2, no. 1, p. 349, 2011.
- [5] L. Lydersen, C. Wiechers, C. Wittmann, D. Elser, J. Skaar, and V. Makarov, "Hacking commercial quantum cryptography systems by tailored bright illumination," *Nature photonics*, vol. 4, no. 10, pp. 686–689, 2010.
- [6] W. Zhang, T. van Leent, K. Redeker, R. Garthoff, R. Schwonnek, F. Fertig, S. Eppelt, W. Rosenfeld, V. Scarani, C. C.-W. Lim, *et al.*, "A device-independent quantum key distribution system for distant users," *Nature*, vol. 607, no. 7920, pp. 687–691, 2022.
- [7] V. Zapatero, T. van Leent, R. Arnon-Friedman, W.-Z. Liu, Q. Zhang, H. Weinfurter, and M. Curty, "Advances in device-independent quantum key distribution," *npj quantum information*, vol. 9, no. 1, p. 10, 2023.
- [8] H.-K. Lo, M. Curty, and B. Qi, "Measurement-device-independent quantum key distribution," *Physical review letters*, vol. 108, no. 13, p. 130503, 2012.
- [9] C. Branciard, E. G. Cavalcanti, S. P. Walborn, V. Scarani, and H. M. Wiseman, "One-sided device-independent quantum key distribution: Security, feasibility, and the connection with steering," *Physical Review A—Atomic, Molecular, and Optical Physics*, vol. 85, no. 1, p. 010301, 2012.
- [10] M. Ioannou, P. Sekatski, A. A. Abbott, D. Rosset, J.-D. Bancal, and N. Brunner, "Receiver-device-independent quantum key distribution protocols," *New Journal of Physics*, vol. 24, no. 6, p. 063006, 2022.
- [11] M. Masini and S. Sarkar, "One-sided di-qkd secure against coherent attacks over long distances," *arXiv preprint arXiv:2403.11850*, 2024.
- [12] C. H. Bennett, G. Brassard, S. Popescu, B. Schumacher, J. A. Smolin, and W. K. Wootters, "Purification of noisy entanglement and faithful teleportation via noisy channels," *Physical review letters*, vol. 76, no. 5, p. 722, 1996.
- [13] I. Devetak and A. Winter, "Distillation of secret key and entanglement from quantum states," *Proceedings of the Royal Society A: Mathematical, Physical and engineering sciences*, vol. 461, no. 2053, pp. 207–235, 2005.
- [14] P. Brown, H. Fawzi, and O. Fawzi, "Device-independent lower bounds on the conditional von neumann entropy," *arXiv preprint arXiv:2106.13692*, 2021.
- [15] P. Brown, H. Fawzi, and O. Fawzi, "Device-independent lower bounds on the conditional von neumann entropy," *Quantum*, vol. 8, p. 1445, 2024.
- [16] M. Navascués, S. Pironio, and A. Acín, "A convergent hierarchy of semidefinite programs characterizing the set of quantum correlations," *New Journal of Physics*, vol. 10, no. 7, p. 073013, 2008.
- [17] W. K. Wootters, "Entanglement of formation of an arbitrary state of two qubits," *Physical Review Letters*, vol. 80, no. 10, p. 2245, 1998.
- [18] C. H. Bennett, G. Brassard, and N. D. Mermin, "Quantum cryptography without Bell's theorem," *Physical Review Letters*, vol. 68, no. 5, pp. 557–559, 1992.
- [19] C. H. Bennett and G. Brassard, "Quantum cryptography: Public key distribution and coin tossing," in *Proceedings of IEEE International Conference on Computers, Systems, and Signal Processing*, pp. 175–179, 1984.
- [20] A. Ali, S. Al-Kuwari, M. Rahim, M. Ghominejad, H. Ali, and S. Hadadi, "A study on thermal quantum resources and probabilistic teleportation in spin-1/2 heisenberg xyz+ dm+ ksea model under variable zeeman splitting," *arXiv preprint arXiv:2405.16294*, 2024.
- [21] H. M. Wiseman, S. J. Jones, and A. C. Doherty, "Steering, entanglement, nonlocality, and the einstein-podolsky-rosen paradox," *Physical review letters*, vol. 98, no. 14, p. 140402, 2007.
- [22] E. G. Cavalcanti, S. J. Jones, H. M. Wiseman, and M. D. Reid, "Experimental criteria for steering and the einstein-podolsky-rosen paradox," *Physical Review A*, vol. 80, p. 032112, 2009.
- [23] M. A. Nielsen and I. L. Chuang, *Quantum computation and quantum information*. Cambridge university press, 2010.
- [24] D. E. Jones, B. T. Kirby, and M. Brodsky, "Tuning quantum channels to maximize polarization entanglement for telecom photon pairs," *npj Quantum Information*, vol. 4, no. 1, p. 58, 2018.
- [25] S. Kucera, C. Haen, E. Arenskötter, T. Bauer, J. Meiers, M. Schäfer, R. Boland, M. Yahyapour, M. Lessing, R. Holzwarth, *et al.*, "Demonstration of quantum network protocols over a 14-km urban fiber link," *npj Quantum Information*, vol. 10, no. 1, p. 88, 2024.
- [26] P. Wittek, "Algorithm 950: Ncpol2sdpa," *ACM Transactions on Mathematical Software*, vol. 41, no. 3, pp. 1–12, 2015.
- [27] MOSEK ApS, "MOSEK optimization toolbox." <https://www.mosek.com/>, 2023.
- [28] C. Simon, M. Afzelius, J. Appel, A. Boyer De La Giroday, S. Dewhurst, N. Gisin, C. Hu, F. Jelezko, S. Kröll, J. Müller, *et al.*, "Quantum memories: a review based on the european integrated project "qubit applications (qap)"", *The European Physical Journal D*, vol. 58, no. 1, pp. 1–22, 2010.
- [29] M. Tomamichel, C. C. W. Lim, N. Gisin, and R. Renner, "Tight finite-key analysis for quantum cryptography," *Nature communications*, vol. 3, no. 1, p. 634, 2012.
- [30] D. V. Reddy, R. R. Nerem, S. W. Nam, R. P. Mirin, and V. B. Verma, "Superconducting nanowire single-photon detectors with 98% system detection efficiency at 1550 nm," *Optica*, vol. 7, no. 12, pp. 1649–1653, 2020.
- [31] D. Deutsch, A. Ekert, R. Jozsa, C. Macchiavello, S. Popescu, and A. Sanpera, "Quantum privacy amplification and the security of quantum cryptography over noisy channels," *Physical Review Letters*, vol. 77, no. 13, pp. 2818–2821, 1996.
- [32] W. Dür, H.-J. Briegel, J. I. Cirac, and P. Zoller, "Quantum repeaters based on entanglement purification," *Physical Review A*, vol. 59, no. 1, p. 169, 1999.